A disposable immunosensor for the detection of salivary MMP-8 as biomarker of periodontitis

Cristina Tortolini[a], Valeria Gigli, Antonio Angeloni[a], Federico Tasca[b], Nguyen T.K. Thanh[c,d], Riccarda Antiochia[e,*]

[a] *Department of Experimental Medicine, Sapienza University of Rome, Viale Regina Elena 324, 00161 Rome, Italy*
[b]*Faculty of Chemistry and Biology, Department of Materials Chemistry, University of Santiago of Chile, Av. Libertador Bernardo O´Higgins 3363, 8320000, Estacion Central, Santiago*
[c]*Biophysics Group, Department of Physics & Astronomy, University College London, Gower Street, London WC1E 6BT, U.K.*
[d]*UCL Healthcare Biomagnetic and Nanomaterials Laboratories, Royal Institution of Great Britain, 21 Albermarle Street, London W1S 4BS, U.K.*
[e]*Department of Chemistry and Drug Technologies, Sapienza University of Rome, P.le Aldo Moro 5, 00185, Rome, Italy*

** Corresponding author.*
E-mail address: riccarda.antiochia@uniroma1.it

ABSTRACT

This work describes the development of a novel voltammetric immunosensor for the detection of salivary MMP-8 at the point-of-care. The electrochemical platform was based on a graphene (GPH) screen-printed electrode (SPE) functionalized by gold-nanospheres (AuNSs) and antibodies against MMP-8 protein (anti-MMP-8). The functionalization with anti-MMP-8 was realized by using 11-mercaptoundecanoic acid (11-MUA), thanks to its ability to give strong sulfur bonds with its -SH end, and to cross-link the $-NH_2$ groups of the antibody molecule with the other -COOH end, using the traditional EDC-NHS method. The voltammetric sensor showed good performances with a linear range of 2.5-300 ng mL^{-1}, a LOD value of 1.0 ± 0.1 ng mL^{-1} and a sensitivity of 0.05 μA mL cm^{-2} ng^{-1}. Moreover, the proposed immunosensor was tested in real saliva samples, showing comparable results to those obtained with the conventional ELISA method. The biosensor was single-use and cost-effective and required a small quantity of test medium and a short preparation time, representing a very attractive biosensor for MMP-8 detection in human saliva.

Keywords

MMP-8; periodontitis; immunosensor; voltammetric biosensor; gold-nanospheres; human saliva.

1. Introduction

Periodontitis is a disease found in the oral cavity which consists of a chronic inflammation of the periodontal tissues, due to the accumulation of dental plaque [1,2]. In the United States, periodontal disease affects about 40% of adults between the ages of 30–80 and about 8% are severely affected [3, 4]. Periodontitis starts as a normal gingivitis and can progress onto a chronic and aggressive disease, with destruction of the periodontal tissue leading to tooth mobility and tooth loss [5].

The concepts of "staging" and "grading", extensively developed in the oncology field, have been adapted to periodontitis [6]. "Staging" relies on the dimensions of the disease severity and complexity of management at presentation, while "grading" refers to the evidence or risk of disease progression. Four stages have been identified, stage I (initial), II (moderate), III (severe) and IV (advanced periodontitis with extensive tooth loss), which correspond to three grades, from grade A (low risk or slow progression) to grade C (high risk or rapid progression) [6].

Mild to moderate chronic periodontitis (grades A and B) is manageable with proper mechanical biofilm and calculus removal, thorough regular oral hygiene checkups, which prevent disease progression. In severe periodontitis (grade C) adequate therapy can no longer prevent tooth loss and it is often associated with potential effects on the systemic health of the patient [7].

Therefore, it is of extreme importance to diagnose chronic periodontitis in its early stages to prevent severe and irreversible tooth damage. As chronic periodontitis is painless during disease progression, it's not common for patients to seek dental treatment in the early stages. Routine diagnostics methods include clinical inspections or X-ray based methods, which may provide information only on tissue destruction and are not useful for prevention and early diagnosis. In this context, the possibility of a non-invasive detection of predictive biomarkers in oral fluids would be a fundamental issue [8].

Matrix metalloproteinase-8 (MMP-8), called also neutrophil collagenase or collagenase 2, has been found as the major metalloproteinase enzyme involved in periodontal disease [9]. MMP-8 belongs to the matrix metalloproteinase family of Zn- and Ca-dependent endo-peptidases, responsible for degradation of extracellular matrix [10,11]. Therefore, the analytical detection of MMP-8 enzyme would enable a reliable quantitative assessment of periodontal "grading", the disease progression key parameter [12].

MMP-8 was demonstrated to be the most prevalent MMP in diseased periodontal tissue, oral fluid, gingival crevicular fluid (GCF) and saliva, whose concentration correlates with disease severity [13]. Various methods have been reported in literature for quantifying MMP-8 in oral fluids, such as enzyme-linked immunosorbent assay (ELISA) [14], time-resolved immunofluorescence assay (IFMA) [24] and lateral-flow immunoassays [15]. The only POC devices for salivary detection of MMP-8 available on the market are PerioSafe ® and Implant Safe ® dipstick immunotests, which combine lateral flow technology with ELISA detection, and are able to distinguish between cases of no/very low risk and cases of elevated risk for periodontal tissue loss, as demonstrated by the study of Nwhator et al., which shows that a lateral-flow neutrophil collagenase- 2 (MMP- 8) immunoassay kit has high sensitivity for periodontitis [16].

Voltammetric immunosensors represent interesting alternatives [17], as they are low cost, sensitive, rapid and easy to use with possibility of POC analysis. They have been recently employed for the detection of 5 out of 23 of the MMPs identified in humans, in particular MMP-1 [18], MMP-9 [19-21], MMP-2 [22-27], MMP-7 [28-32] and MMP-3 [33].

To improve the sensitivity and selectivity of biosensors, nanomaterial-based platforms have been used, in particular graphene has attracted particular interest thanks to its unique electronic properties [34]. Moreover, combined with metallic nanoparticles, the intrinsic electrocatalytic activity of graphene resulted greatly enhanced through nanoparticle electronic structure modification, thus providing a better electron transfer pathway [35].

In this work, we describe the development of a voltammetric immunosensor for the detection of MMP-8 protein in saliva using specific MMP-8 antibodies immobilized on a AuNSs/GPH screen printed electrode. The obtained AuNSs/GPH nanocomposite not only increased the surface area to bind larger amounts of antibody, but also promoted efficient electron transfer for improved biosensing electrochemical performances. The immunosensor was tested on saliva samples showing very good agreement with the results obtained with the standard ELISA assays and a significant correlation with the classical clinical parameters of periodontitis allowing to distinguish between the different stages of the disease and to evaluate the efficacy of treatment. To the best of our knowledge this is the very first time that a voltammetric immunosensor has been developed and applied for MMP-8 detection.

2. Experimental

2.1. Materials

MMP-8, MMP-2 and MMP-9 Proteins were purchased from AnaSpec (Fremont, USA) and MMP-8 antibody (B-1) (anti-MMP-8) from Santa Cruz Biotechology, Inc.
All chemicals used were analytical grade and used without any further purification: sodium monobasic phosphate (Na_2HPO_4), sodium dibasic phosphate (NaH_2PO_4), potassium chloride (KCl), potassium ferricyanide (III) ($K_3[Fe(CN)_6]$), potassium ferrocyanide (II) ($K_4[Fe(CN)_6]$, (N-(3-dimethylaminopropyl)-N′-ethylcarbodiimide hydrochloride, commercial grade (EDC) and N-hydroxysuccinimide, 98% (NHS), 11-Mercaptoundecanoic acid (11-MUA), ethanol, ≥ 98%, Bovine Serum Albumin (BSA), glucose, urea, uric acid, amylase, SP-A and SP-B purchased from Sigma-Aldrich (Buchs, Switzerland).

All solutions were prepared in phosphate buffer 0.1 M, KCl 0.1 M, pH 7.4 (PBS buffer). A solution of 1.1 mM $K_3[Fe(CN)_6$ and 0.1 M KCl in water was used in cyclic voltammetric experiments for determination of electroactive area (A_e) using the Randles–Ševcik equation. High-purity deionized water (resistance: 18.2 MΩ cm at 25 °C; TOC < 10 µg L^{-1}) obtained from Millipore (Molsheim, France) was used throughout experiments.

2.2. Apparatus and electrochemical measurement

The size and shape of AuNSs were examined by transmission electron microscopy (TEM) and scanning electron microscopy (SEM) analysis. TEM was performed on a JEOL 1200 EX2 (JEOL USA, Massachusetts, USA) operating with an acceleration voltage of 150 kV. The size of the AuNPs was determined using ImageJ software25 on at least 10 TEM images. Samples for TEM examination were prepared by drop-casting of 10 µL of AuNPs solution onto a Carbon Film on Mesh Copper (C200Cu, EMR Resolutions, Sheffield, UK) and left to dry for 24 hours.
SEM and energy-dispersive X-ray spectroscopy analysis (EDX) measurements were performed with High-Resolution Field Emission Scanning Electron Microscopy (HR FESEM, Zeiss Auriga Microscopy, Jena, Germany).
UV-Visible spectra were recorded on a SpectraMax M2e spectrophotometer (Molecular Devices, Workingham RG41 5TS, UK) with samples (3 mL of AuNPs solution in water) contained in Polystyrene Macro Cuvettes (Fisherbrand™, capacity 4mL), operating at a resolution of 1 nm from 400 to 700 nm for AuNSs. The blank was carried out in Milli-Q water. The data were successively analyzed with the SoftMax Pro software.
Raman measurements were recorded using iRaman plus, model BWS465-785S (B&WTek) at λ=785 nm, with a probe laser power of 340 mW and using a detector High Quantum Efficiency CCD Array. All electrochemical measurements were carried out in a 10 mL thermostated glass cell (model 6.1415.150, Metrohm, (Herisau, Switzerland) with a conventional three-electrode configuration consisting of an Ag/AgCl/KCl_{sat} (198 mV vs. NHE), as reference electrode (cat. 6.0726.100, Metrohm, Herisau, Switzerland), a glassy carbon rod as counter electrode (cat. 6.1248.040, Metrohm, Herisau, Switzerland) and a graphene screen-printed electrode (diameter 3 mm, 110GPH, GPH,

Metrohm, Herisau, Switzerland) as a working electrode, respectively. A graphene-gold nanoparticles dual screen-printed carbon electrode (diameter 3 mm, C1110GPH-GNP, Metrohm, Herisau, Switzerland) was used as comparison.
All electrochemical measurements were recorded using freshly prepared in 5 mM solution of ferrocyanide/ferricyanide $[Fe(CN)_6]^{3-/4-}$ 1.1 ratio, in PBS pH=7.4 (Zobell's solution) [36].
DPV measurements were recorded by scanning from -0.1 to 0.6 V, amplitude 20 mV and step potential 5 mV. Base-line corrections were done for all DPV data using the NOVA software.
EIS experiments were carried out at equilibrium potential called open circuit potential (OCP) without bias voltage in the frequency range of 0.1-10^5 Hz (MWCNTs SPE electrodes), using an ac signal of 10 mV amplitude at the formal potential of the redox probe (0.2 V vs Ag/AgCl) using Autolab Potentiostat/Galvanostat (Eco Chemie, The Netherlands).
Electrochemical measurements were performed in a glass cell (model 6.1415.150, Metrohm, Herisau, Switzerland) with a conventional three-electrode configuration with an Ag/AgCl/KCl_{sat} (198 mV vs. NHE) as a reference electrode (cat. 6.0726.100, Metrohm, Herisau, Switzerland), a glassy carbon rod as a counter electrode (cat. 6.1248.040, Metrohm, Herisau, Switzerland).
The saliva samples protocol is as follows: incubation of the sample (10 µL, on the working electrode) for 10 min, washing with PBS buffer for about 30 seconds and drop-casting of 40 µL of Zobell's solution on SPE.

2.3. Synthesis of AuNSs

The gold nanospheres (AuNSs, diameter 18 nm) were synthesized according to a slightly modified procedure reported in our previous work [37,38]. In a two necked 250 mL flask with condenser, 125 mL of a 254 µM $HAuCl_4$ solution were heated at strong reflux under vigorous stirring (oil bath temperature 156 °C). When the reflux was stable, 12.5 mL of a 40 mM sodium citrate solution in water was added to the reaction flask. After few minutes the solution turned wine red and it was kept under stirring for other 10 min. After the synthesis of the AuNPs the solution obtained was centrifuged and the AuNSs were resuspended in water and sonicated for 5 minutes.

2.4. Preparation of anti-MMP-8/11-MUA/AuNSs/GPH/SPE immunosensor

The modified sensors were assembled by the following method: firstly, 10 µL of AuNSs solution were drop-casted on the working electrode and let dry at room temperature (RT). Then, the SPE was immersed in freshly prepared 5 mM 11-MUA in ethanolic solution overnight. The modified electrode was rinsed with ethanol to remove any unbound molecules.
Successively, the antibody was immobilized onto the surface by EDC/NHS cross-linking chemistry by drop-casting a mixture of 3 µL of EDC solution (0.5 mM in PBS 0.1 M, pH 7.2, KCl 0.1 M) and 3 µL of NHS solution (0.1 mM in PBS 0.1 M, pH 7.2, KCl 0.1 M) for 30 min, according to a procedure reported by Gigli et al. [39]. The sensor was then immersed in BSA solution (10 µL, 0.25% w/v) for 15 min, as blocking agent, to avoid non-specific interactions. The surface electrode was washed by buffer solution at the end of each fabrication step and stored at 4 °C before use.

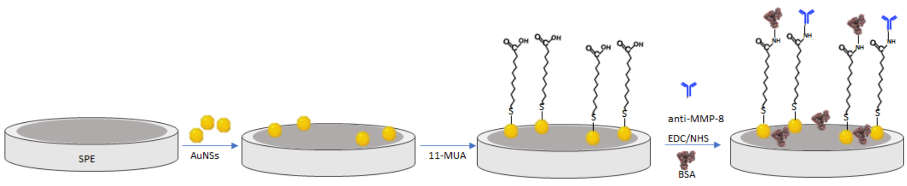

Scheme 1. Preparation of modified GPH-SPE by AuNSs deposition, 11-MUA SAM formation, BSA surface blocking and antibody coupling by EDC/NHS cross-linking chemistry.

2.5. Collection and preparation of human saliva samples

Unstimulated saliva samples were collected by direct expectoration of the patients into plastic tubes (1 mL), centrifuged for 10 min at 1500 g at 4 °C and then used for measurements. Samples not immediately tested are stored at -80 °C. Volunteers are only asked to drink a glass of water before saliva collection, to match the requirement of a POC device.

3. Results and Discussion

3.1. TEM and SEM characterization

TEM and SEM measurements were performed in order to characterize shape, dimensions and size distributions of AuNSs. Figures 1 A, B, C, D and E show Au nanoparticles with spherical form, homogeneous size distribution and crystalline structure without aggregates and clusters. The average diameter of the AuNSs resulted to be 18.9 nm.

EDX experiments (Figures 1 F, G) show the elemental mapping analysis of the AuNSs, confirming the presence of the Au atom in the scanned electron micrograph image and therefore the effective immobilization of the AuNSs on the electrode surface.

3.2. UV-VIS characterization

The size of the particles was further confirmed by UV-VIS spectrum that showed a strong absorption band at about 520 nm (Fig. 2). This result is in good agreement with λ values reported in literature for AuNPs with a diameter of about 20 nm [40,41], as it is well-known that the SPR band shows a λ shift between 515 and 530 nm at increasing AuNPs diameter from 5 to 40 nm.

3.3. Raman characterization

Raman spectroscopy has been used to investigate the features of the nano-modified graphene, based on the change in frequency of photons. Figure 3 shows the Raman spectra of GPH and AuNSs/GPH screen-printed electrodes. Both samples showed the characteristic D band at about 1350 cm^{-1}, corresponding to defects in graphene surface, and G band at about 1525 cm^{-1}, corresponding to the optical mode vibrations of sp^2 bonded carbon atoms. An enhancing effect of the Raman signals of graphene can be observed after the modification of the electrode surface with AuNSs and the I_D/I_G ratio decreases substantially (from 0.83 to 0.66), pointing out increased defects in the graphene network due to the presence of gold atoms which act as defect sites.

3.4. Electrochemical characterization of MMP-8 immunosensor platform

Characterization of each modification step of the immunosensor surface was performed using CV, DPV and EIS measurements, utilizing a 5 mM of $[Fe(CN)_6]^{3-/4-}$ redox couple solution.

3.4.1. CV and DPV characterization

Fig. 4A shows the CVs curves after each modification step. Two reversible well-defined redox peaks, due to the oxidation/reduction of ferricyanide, are clearly visible on both bare GPH/SPE (black curve) and AuNSs/GPH/SPE (red curve) electrode, with a marked increase of the peak currents in the last case. This electrochemical behavior is well-known in literature and is due to the increase of the electrical conductivity of the electrode surface after AuNSs immobilization, thanks to the increased electroactive area and the better electron transfer-promoting features of the gold nanomaterial.
It is interesting to note that the peak currents obtained with AuNSs are higher than that obtained with the commercial GNPs/GPH/SPE (green curve), indicating the superior electrochemical performances of the NSs, in terms of better conductivity allowing a faster electron transfer between ferricyanide and the electrode surface.
However, a clear decrease of the redox current is observed after immobilizing 11-MUA SAM (11-MUA/AuNSs/GPH/SPE, blue curve), and a further decrease after the immobilization of the antibody in addition with BSA (anti-MMP-8/BSA/11-MUA/AuNSs/GPH/SPE electrode, pink curve) on the electrode surface. Furthermore, a significant decrease of the electrochemical reversibility is registered with anodic and cathodic peak potentials shifted to more positive and negative potentials, respectively, with corresponding larger ΔEp values. Table 1 shows all electroanalytical parameters before and after the modification steps, such as ΔEp, electroactive area (A_e), roughness factor (ρ) and the heterogeneous transfer rate constant (k_0). The A_e values have been calculated by using the following Randles-Sevcik equation for a reversible process [42]:

$$I_p = 2.686 \times 10^5 \, n^{3/2} A_e D_0^{1/2} C_0 \upsilon^{1/2} \quad (1)$$

where Ip=the peak current, n=number of electrons ($n = 1$), Ae=electroactive area (cm^2), D_0= diffusion coefficient (7.6×10^{-6} cm^2 s^{-1} for $Fe(CN)_6]^{3-/4-}$), C_0=concentration (mol cm^{-3}), and υ=scan rate (Vs^{-1}). The A_e values have been evaluated by using the I_p vs $\upsilon^{1/2}$ slope for each electrode, k_0 values by using the merged Klingler-Kochi/Nicholson-Shain method [43,44], and ρ from the Ae/Ag ratio for each electrode, where Ag is the geometric area of the electrode.
The calculated k_0 values agree with the ΔEp data pattern. Larger ΔEp correspond to a lower electron transfer kinetics of the redox probe (lower k_0 values), due to the blocking effect caused by the immobilized layers of 11-MUA-SAM, and anti-MMP-8/BSA. In particular, the formation of the MMP-8/antibody complex on the electrode surface caused the interface to severely block the electrochemistry of $[Fe(CN)_6]^{3-/4-}$ with a significant reduction of the electron transfer rate of the redox probe from $(2.68 \pm 0.21) \times 10^{-3}$ cm s^{-1} to (1.59 ± 0.19) 10^{-3} cm s^{-1}.
These results clearly attest the effective covalent immobilization of both 11-MUA SAM and anti-MMP-8 antibody. Firstly, a thiol functionalized gold (Au-S bond) between Au atoms of AuNSs and the S-atom of the SAM is generated by the 11-MUA molecule. Then, the terminal -COOH of 11-MUA, activated by the EDC/NHS forming a typical NHS-ester, formed a very strong covalent

Commented [RA1]:

Commented [RA2]:

"amidic" linkage with the amino group of the antibody molecule, thus hampering the electron-transfer kinetics of $[Fe(CN)_6]^{3-/4-}$ at the electrode/electrolyte interface.
It is interesting to note that the peak current reduction observed for the pink curve in Fig. 5 is partially due to the insulating BSA molecule, immobilized together with the antibody as blocking agent of the non-binding sites at the biosensor surface.
The same electrochemical behavior is observed with DPV curves (Fig. 4B), confirming the results obtained with CVs experiments.

3.4.2. EIS characterization

To assess the effectiveness of the AuNSs immobilization as well as the antibody binding by SAM technique, electrochemical impedance spectroscopy (EIS) experiments were also performed, by measuring the impedance difference between bare, AuNSs modified, SAM modified and antibody-bonded SAM electrode.
Fig. 5 shows the Nyquist plots of GPH bare, AuNSs-GPH, 11-MUA/AuNSs/GPH and anti-MMP-8/11-MUA/AuNSs/GPH screen printed electrode. The semicircle diameter of the Nyquist plot obtained with AuNSs is smaller than the bare electrode, confirming the excellent conductivity of the nanomaterial, which results strongly immobilized onto the electrode surface, resulting in a faster electron-transfer kinetics of the redox probe. After the binding of 11-MUA and anti-MMP-8 a progressive increase in the semicircle diameter has been observed (blue and pink curves), due to the hampering effect of both immobilized molecules on the charge transfer.
The impedance spectra were fitted by a simple Randles circuit [R(Q[RW])] (Fig. 5, inset) in order to obtain the charge transfer resistance (R_{CT}) values, corresponding to the semicircle of the Nyquist plot, the constant phase element and the Warburg constant values (Table 2). The R_{CT} values confirmed the trend of the Nyquist plot with an initial decrease after electrode modification with AuNSs and a successive large increase after 11-MUA and antibody immobilization, responsible for the hindering of the electron transfer between the redox probe and the electrode surface.
The results obtained by EIS characterization perfectly agreed with those obtained with CV and DPV reported above.
In order to demonstrate the efficacy of the antibody binding by SAM technique compared to physical adsorption, EIS experiments were conducted also in absence of immobilized 11-MUA SAM after 8 h of physical immersion in an anti-MMP-8 solution. The R_{CT} values for physically adsorbed and self-assembled monolayer (SAM) of anti-MMP-8 are reported in Figure S1 in absence and in presence of MMP-8 molecule. The results demonstrated that a lower R_{CT} values is obtained without SAM technique due to the presence of less immobilized molecules of anti-MMP-8 on the electrode surface. However, the physically adsorbed anti-MMP-8 was not sufficient to show any variation of the R_{CT} signal in presence of MMP-8 molecule. This can be ascribed to the random orientation of the antibody adsorbed onto the electrode surface, whereas there is a higher probability that the SAM-linked antibody is proper-oriented for MMP-8 binding. In this case, the amino groups involved in the covalent attachment (amidic bond) may irreversibly fix the MMP-8 antibodies allowing a "Fab accessible" orientation for the successive MMP-8 binding.

3.5. Optimization studies of MMP-8 immunosensor platform

Optimization studies were carried out on the concentration of immobilized MMP-8 antibody and its binding time on the modified electrode surface by DPV technique.
The current density reached a minimum value, attesting saturation of the electrode surface, at an antibody concentration of 40 μg mL^{-1} and with a binding time of 20 min (Fig. S2A and B) and therefore these values were chosen for further experiments.

DPV experiments were also used to investigate the optimum incubation time of MMP-8 for different time periods between 1 and 30 minutes. At an incubation time of 10 minutes the current response reached a plateau (Fig. S2C), demonstrating the reaching of the electrode surface saturation for the optimized antibody concentration.

3.6. Analytical performances of MMP-8 immunosensor

Under the optimal conditions, DPV technique has been used to construct the calibration plot of the MMP-8 immunosensor obtained with MMP-8 concentrations in the range 2.5-500 ng mL^{-1} in PBS pH=7.4 using $[Fe(CN)_6]^{3-/4-}$ as redox probe. When MMP-8 is exposed to the anti-MMP-/11-MUA/AuNSs/GPH/SPE biosensor, a blocking effect is observed by the progressive peak currents decrease due to the formation of MMP-8-bound antibodies at the sensing interface, creating a substantial barrier to $[Fe(CN)_6]^{3-/4-}$ electron transfer kinetics. As shown in Fig. 6, the current density resulted linear with MMP-8 concentration in the range 2.5-500 ng mL^{-1}, with a detection limit of 1 ng/ml, calculated with the formula $3\sigma/S$, with σ the standard deviation of the intercept and S the slope of the calibration plot, and a sensitivity of 0.05 μA mL cm^{-2} ng^{-1}. The corresponding linear regression equation resulted to be y= 0.05x+11.57 with an R^2 value of 0.986 (n=3, RSD < 4%).
The reproducibility of the biosensor was investigated by analyzing DPV response of one MMP-8 level for ten replicate measurements with the same immunosensor and the repeatability was also estimated by measuring one MMP-8 level with ten different immunosensors realized according to the same electrode modifying procedure, independently. All biosensors were incubated with 50 ng mL^{-1} MMP-8 in Zobell's solution. The relative standard deviation (RSD) of the intra- and inter-assay resulted to be 7.1% and 6.3%, implying acceptable reproducibility and repeatability of the proposed biosensor.
Furthermore, about 90% of the DPV response of the biosensor to 50 ng mL^{-1} MMP-8 was maintained when the biosensor is kept at 4°C for 2 weeks, indicating a desired storage stability of the proposed MMP-8 biosensor.
Table 3 shows a brief overview of the electrochemical biosensors reported in literature for measuring different MMPs [19-33, 45-56]. Our results are consistent with these works but show higher LOD values. However, the linear range of our biosensor is within the clinically relevant range of MMP-8 and therefore it can be a potential useful tool for POC diagnosis of periodontal disease. The only biosensor reported in literature for MMP-8 detection is based on piezoelectric surface acoustic wave (SAW) technology. The analytical performances are reported in the last row of Table 3. In this case the biosensor shows a more extended linear range (up to 1000 ng mL^{-1}) but a higher LOD (62.5 ng mL^{-1}) [57].

3.7. Selectivity studies

Cross-reactivity studies were performed to evaluate the effects of possible interfering substances in real saliva samples and to assess the selectivity of the method. Glucose, urea, uric acid, amylase, SP-A and SP-B and the two gelatinase enzymes of the MMP family, namely MMP-2 and MMP-9, which seem to have a role in chronic periodontitis, have been tested. In healthy people, the concentration of glucose in saliva ranges from 5-10 ng mL^{-1}, thus a concentration of 50 ng mL^{-1}, much higher than in human body, has been selected, while a concentration of 250 ng mL^{-1} was selected for all other potential interferents, 10-times higher than the concentration of MMP-8 used in the test (25 ng mL^{-1}). Compared with the target analyte, this method showed almost negligible current signal for the other non-target analytes, although the higher concentrations were employed (Fig. 7). These results clearly indicate no cross-reactivity event against the MMP-8 protein tested.
Table S1 shows the alignment sequence between MMP-8, MMP-2 and MMP-9 and a target sequence obtained from the manufacture's technical support, indicating the binding region of MMP-8 to the

antibody. The sequence identity for MMP-2 and MMP-9 is less than 50%, with a positivity index for MMP-2 slightly higher than for MMP-9, resulting 60% and 58%, respectively.
Structural overlap analysis showed that both MMP-2 and MMP-9 present a similar secondary structure of the target compared to MMP-8, although the different amino acid composition of the target region (Fig. 8). The target (red color) is localized in the same portion for MMP-8 (green) and MMP-2 (cyano), whereas for MMP-9 (magenta) is in a different portion. These results may explain the low selectivity of the antibody towards MMP-2 and especially MMP-9, as reported above.

3.8. Application in real saliva samples

The efficiency of the proposed immunosensor was assessed using saliva samples of 10 volunteers, in particular: 5 healthy individuals, 3 affected by gingivitis and 2 by chronic periodontitis.
The human saliva samples were used directly after collection by simple drop-casting onto the electrode surface (10 μL) after 1:2 dilution in water. The results obtained with the biosensor were compared to the conventional ELISA method and are shown in Table 4. A good agreement between the two methods (RSD% values between 4.7 and 12.4) is observed, indicating a satisfactory accuracy, suggesting the possible use of the proposed immunosensor in the assay of MMP-8 in human saliva samples. It is interesting to note that higher salivary MMP-8 levels are detected in individuals affected by gingivitis and periodontitis compared to healthy participants, although cut-off values have not been reported in literature [14]. The results were also compared with Periosafe ® kit (Dentognostics GmbH, Jena, Germany), the commercially available active MMP-8 lateral-flow POC immunotest, which combines lateral flow technology with ELISA detection [8,57]. The cut off value of Periosafe test is 25 ng mL^{-1} in 5 mL mouth rinse samples (3-4 drops of oral rinse), which corresponds to the presence of a light line on the test stick (positive test). Moreover, the color intensity of the line indicates the level of risk: a light line corresponds to low risk, a dark line to high risk.

4. Conclusions

By immobilizing AuNSs onto a graphene SPE and after its proper functionalization with SAM technique, we developed a promising immunosensor for fast and sensitive detection of MMP-8 in human saliva. The decrease in the voltammetric current and the increase in the R_{CT} values demonstrated that functionalization was successful. The new AuNSs based immunosensor is sensitive to concentrations of MMP-8 as low as 1 ng mL^{-1}, with a linear range between 2.5 and 500 ng/mL and a sensitivity of 0.05 μA mL cm^{-2} $ng^{-}1$, comparable to ELISA assay. However, the new device is much simpler to perform, faster and cheaper. Although gold is quite expensive, the total cost of the biosensor is low (around $5/sensor), as small amounts of AuNSs are employed. The biosensor showed also good selectivity, reproducibility and stability.
Furthermore, regarding potential clinical relevance and practical advantages, the proposed biosensor represents a promising tool for non-invasive screening of periodontitis at the POC/chairside. The biosensor may be useful for prediction of risk of periodontal disease or periodontal disease progression and reflects also the therapeutic response. Thanks to its high sensitivity and selectivity, it is able to differentiate between periodontal health, gingivitis and the different stages of periodontitis. Of course, there is a wide inter-subject variability in the MMP-8 salivary concentrations [58], which still makes correlations difficult and may affect the diagnosis. Therefore, more studies and randomized designs with larger number of samples are still needed in order to develop affordable criteria and "cut-off" value for clinical association of measured MMP-8 levels with periodontal health status as well as with other chronic conditions, such as diabetes and cardiovascular diseases, which recent studies [3] demonstrated to be correlated to high MMP-8 levels. The knowledge of the relationship between salivary MMP-8 biomarker and oral- and systemic diseases is still in its infancy and additional work is still required for an accurate use of MMP-8 levels as prognostic value.

Acknowledgments

The authors thank Metrohm Italiana srl for the optimization of the Raman Measurements and Dr. Flavio Rizzo for molecular docking studies.

Supplementary Materials: Figure S1. R_{CT} values for immobilized anti-MMP-8 and MMP-8-bound anti-MMP-8 based on physically adsorbed and 11-MUA SAM on AuNSs-GPH-SPE; Figure S2. Optimization of anti-MMP-8 antibody concentration (A), anti-MMP-8 binding time (B) and (C) MMP-8 incubation time. Experimental conditions: (A) 3 µL of different anti-MMP-8 concentrations on the working electrode of anti-MMP-8/EDC-NHS11-/MUA/AuNSs/GPH/SPE, for 20 min antibody immobilization time, measured in 50 µL of Zobell's solution; (B) 3 µL of 20 µg/mL of anti-MMP-8, for different binding times; (C) 4 µL of MMP-8 incubated for different times on anti-MMP-8/EDC-NHS/11-MUA/AuNSs/GPH/SPE measured in 50 µL of Zobell's solution. Three replicates for each condition have been carried out (n=3); Table S1. Sequence alignment of human MMP-8, MMP-2 and MMP-9 with Target. Target is an amino acids 122-166 mapping within an internal region of MMP-8 of human origin.

Author Contributions: Conceptualization: R.A.; investigation: C.T., V.G.; methodology: C.T., V.G., F.T.; visualization: V.G.; resources: A.A.; data curation: C.T., F.T.; writing-original draft preparation: R.A., N.T.; supervision: R.A. All authors have read and agreed to the published version of the manuscript.

Funding: This work was supported by the Italian Ministry of Education, Universities, and Research (Progetto di Ateneo 2022, No. RP12117A8B0CA73F).

Institutional Review Board Statement: Not applicable.

Informed Consent Statement: Not applicable.

Data Availability Statement: Not applicable.

Conflicts of Interest: The authors declare no conflict of interest.

References

[1] P.N. Papapanou, Periodontal diseases: epidemiology, Ann Periodontol 1 (1996) 1–3, https://doi.org/10.1902/annals.1996.1.1.1.

[2] G.C. Armitage, The complete periodontal examination, Periodontol 2004 (2000) 22–33, https://doi.org/10.1046/j.0906-6713.2002.003422.x.

[3] L. Steigmann, S. Maekawa, C. Sima, S. Travan, C.W. Wang, W.V. Giannobile, Biosensor and lab-on-a-chip biomarker-identifying technologies for oral and periodontal diseases, Front Pharmcol 11 (2020) 588480, https://doi.org/10.3389/fphar.2020.588480.

[4] P.I. Eke, G.O. Thornton-Evans, L. Wei, W.S. Borgnakke, B.A. Dye, R.G. Genco, Periodontitis in US adults: National Health and Nutrition Examination Survey 2009-2014, J Am Dent Assoc 149 (2018) 576–588, https://doi.org/10.1016/j.adaj.2018.04.023.

[5] G.C. Armitage, Development of a classification system for periodontal diseases and conditions, Ann Periodontol 4 (1999) 1–6, https://doi.org/10.1902/annals.1999.4.1.1.

[6] M.S. Tonetti, H. Greenwell, K.S Kornman, Staging and grading of periodontitis: Framework and proposal of a new classification and case definition, J Clin Periodontol 45 (2018) S149–S161, https://doi.org/10.1002/jper.18-0006.

[7] J. Lindhe, R. Ranney, I. Lamster, A. Charles, C.P. Chung, T. Flemmig, D. Kinane, M. Listgarten, H. Löe, R. Schoor, G. Seymour, M. Somerman, Consensus report: chronic periodontitis, Ann Periodontol 4 (1999) 1–38, https://doi.org/10.1902/ANNALS.1999.4.1.38.
[8] E.F. de Morais, J.C. Pinheiro, R.B. Leite, P.P.A. Santos, C.A.G. Barboza, R.A. Freitas, Matrix metalloproteinase-8 levels in periodontal disease patients: A systematic review, J Periodont Res 53 (2018) 156–163, https://doi.org/10.1111/jre.12495.
[9] S.I. Borujeni, M. Mayer, P. Eickholz, Activated matrix metalloproteinase-8 in saliva as diagnostic test for periodontal disease? A case- control study, Med Microbiol Immunol 204 (2015) 665–672, https://doi.org/10.1007/s00430-015-0413-2.
[10] T. Sorsa, P. Mäntylä, T. Tervahartiala, P.J. Pussinen, J. Gamonal, M. Hrnandez, MMP activation in diagnostics of periodontitis and systemic inflammation, J Clin Periodontol 38 (2011) 817–819, https://doi.org/10.1111/j.1600-051x.2011.01753.x.
[11] T. Sorsa, L. Tjäderhane, Y.T. Konttinen, Matrix metalloproteinases: contribution to pathogenesis, diagnosis and treatment of periodontal inflammation, Ann Med 38 (2006) 306–321, https://doi.org/10.1080/07853890600800103.
[12] T. Sorsa, S. Alassiri, A. Grigoriadis, I.T. Räisänen, P. Pärnänen, S.O. Nwhator, D.R. Gieselmann, D. Sakellari, Active MMP-8 (aMMP-8) as a grading and staging biomarker in the periodontitis classification, Diagnostics 10 (2020) 61, https://doi.org/10.3390/diagnostics10020061.
[13] N. Gupta, N.D. Gupta, A. Gupta, S. Khan, N. Bansal, Role of salivary matrix metalloproteinase-8 (MMP-8) in chronic periodontitis diagnosis, Front Med 9 (2015) 72–76, https://doi.org/10.1007/s11684-014-0347-x.
[14] K.A. Umeizudike, H. Lähteenmäki, I.T. Räisänen, J.J. Taylor, P.M. Preshaw, S.M. Bissett, T. Tervahartiala, S.O. Nwhator, P. Pärnänen, T. Sorsa, Ability of matrix metalloproteinase-8 biosensor, IFMA, and ELISA immunoassays to differentiate between periodontal health, gingivitis, and periodontitis, J Periodontal Res 57 (2022) 558–567, https://doi.org/10.1111%2Fjre.12985.
[15] N. Johnson, J.L. Ebersole, R.J. Kryscio, R.J. Danaher, D. Dawson, M. Al-Sabbagh, C.S. Miller, Rapid assessment of salivary MMP-8 and periodontal disease using lateral flow immunoassay, Oral Dis 22 (2016) 681–687, https://doi.org/10.1111/odi.12521.
[16] S.O. Nwhator, P.O. Ayanbadejo, K.A. Umeizudike, O.I. Opeodu, G.A. Agbelusi, J. Olamijulo, M.O. Arowojolu, T. Sorsa, B.S. Babajide, D.O. Opedun, Clinical correlates of a lateral- flow immunoassay oral risk indicator, J Periodontol 85 (2014) 188–194, https://doi.org/10.1902/jop.2013.130116.
[17] A. Kirchhain, N. Poma, P. Salvo, L. Tedeschi, B. Melai, F. Vivaldi, A. Bonini, M. Franzini, L. Caponi, A. Tavanti, F. Di Francesco, Biosensors for measuring matrix metalloproteinases: An emerging research field, TrAC Trends in Anal Chem 110 (2019) 35–50, https://doi.org/10.1016/j.trac.2018.10.027.
[18] X. Liu, L. Lin, F. Tseng, Y. Tan, J. Li, L. Feng, L. Song, C. Lai, X. Li, R. He, Label-free electrochemical immunosensor based on gold nanoparticle/polyethyleneimine/reduced graphene oxide nanocomposite for the ultrasensitive detection of cancer biomarker matrix mettaloproteinase-1, Analyst 146 (2021) 4066–4079, https://doi.org/10.1039/D1AN00537E.
[19] D.S. Shin, Y. Liu, Y. Gao, T. Kwa, Z. Matharu, A. Revzin, Micropatterned surfaces functionalized with electroactive peptides for detecting protease release from cells, Anal Chem 85 (2013) 220–227, https://doi.org/10.1021/ac302547p.
[20] A. Biela, M. Watkinson, U.C. Meier, D. Baker, G. Giovannoni, C.R. Becer, S. Krause, Disposable MMP-9 sensor based on the degradation of peptide cross-linked hydrogel films using electrochemical impedance spectroscopy, Biosens Bioelectron 68 (2015) 660–667, https://doi.org/10.1016/j.bios.2015.01.060.
[21] H. Park, H. Lee, S.H. Jeong, E. Lee, W. Lee, N. Liu, D.S. Yoon, S. Kim, S.W. Lee, MoS_2 Field-Effect Transistor-Amyloid-β_{1-42} Hybrid Device for Signal Amplified Detection of MMP-9, Anal Chem 91 (2019) 8252–8258, https://doi.org/10.1021/acs.analchem.9b00926.

[22] P. Jing, H. Yi, S. Xue, R. Yuan, W. Xu, A 'signal on-off' electrochemical peptide biosensor for matrix metalloproteinase 2 based on target induced cleavage of a peptide, RSC Adv. 5 (2015) 65725–65730, https://doi.org/10.1039/C5RA10662A.
[23] D. Wang, Y. Yuan, Y. Zheng, Y. Chai, R. Yuan, An electrochemical peptide cleavage-based biosensor for matrix metalloproteinase-2 detection with exonuclease III-assisted cycling signal amplification, Chem Commun 52 (2016) 5943–5945, https://doi.org/10.1039/C6CC00928J.
[24] W. Xu, P. Jing, H. Yi, S. Xue, R. Yuan, Bimetallic Pt/Pd encapsulated mesoporous-hollow CeO_2 nanospheres for signal amplification toward electrochemical peptide-based biosensing for matrix metalloproteinase 2, Sensor Actuator B Chem 230 (2016) 345-352, https://doi.org/10.1016/j.snb.2016.02.064.
[25] B.B. Kou, Y.Q. Chai, Y.L. Yuan, R. Yuan, PtNPs as scaffolds to regulate interenzyme distance for construction of efficient enzyme cascade amplification for ultrasensitive electrochemical detection of MMP-2, Anal Chem 89 (2017) 9383–9387. https://doi.org/10.1021/acs.analchem.7b02210.
[26] T. Zheng, R. Zhang, Q. Zhang, T. Tan, K. Zhang, J.J. Zhu, H. Wang, Ultrasensitive dual-channel detection of matrix metalloproteinase-2 in human serum using gold-quantum dot core–satellite nanoprobes, Chem Commun 49 (2013) 7881–7883, https://doi.org/10.1039/C3CC44623A.
[27] J.H. Choi, H. Kim, H.S. Kim, S.H. Um, J.W. Choiand, B.K. Oh, MMP-2 Detective silicon nanowire biosensor using enzymatic cleavage reaction, J Biomed Nanotechnol 9 (2013) 732–735, https://doi.org/10.1166/jbn.2013.1541.
[28] G. Liu, J. Wang, D.S. Wunschel, Y. Lin, Electrochemical proteolytic beacon for detection of Matrix Metalloproteinase activities, J Am Chem Soc 128 (2006) 12382–12383, https://doi.org/10.1021/ja0626638.
[29] Y. Zheng, Z. Ma, Dual-reaction triggered sensitivity amplification for ultrasensitive peptide-cleavage based electrochemical detection of matrix metalloproteinase-7, Biosens Bioelectron 108 (2018) 46–52, https://doi.org/10.1016/j.bios.2018.02.045.
[30] D. Wang, Y. Chai, Y. Yuan, R. Yuan, A Peptide cleavage-based ultrasensitive electrochemical biosensor with an ingenious two-stage DNA template for highly efficient DNA exponential amplification, Anal Chem 89 (2017) 8951–8956, https://doi.org/10.1021/acs.analchem.7b01477.
[31] B.B. Kou, L. Zhang, H. Xie, D. Wang, Y.L. Yuan, Y.Q. Chai, R. Yuan, DNA Enzyme-decorated DNA nanoladders as enhancer for peptide cleavage-based electrochemical biosensor, ACS Appl Mater Interfaces 8 (2016) 22869–22874, https://doi.org/10.1021/acsami.6b07017.
[32] H. Chen, P. Chen, J. Huang, R. Selegård, M. Platt, A. Palaniappan, D. Aili, A.I.Y. Tok, B. Liedberg, Detection of Matrilysin activity using polypeptide functionalized reduced Graphene oxide Field-Effect Transistor sensor, Anal Chem 88 (2016) 2994–2998, https://doi.org/10.1021/acs.analchem.5b04663.
[33] B.S. Munge, J. Fisher, L.N. Millord, C.E. Krause, R.S. Dowd, J.F. Rusling, Sensitive electrochemical immunosensor for matrix metalloproteinase-3 based on single-wall carbon nanotubes, Analyst (2010) 135 1345–1350, https://doi.org/10.1039/C0AN00028K.
[34] X. Huang, Z.Y. Zeng, Z.X. Fan, J.Q. Liu, H. Zhang, Graphene-based electrodes, Adv. Mater. 24 (2012) 5979–6004, https://doi.org/10.1002/adma.201201587.
[35] L. Fritea, F. Banica, T.O. Costea, L. Moldovan, L. Dobjanschi, M. Muresan, S. Cavalu, Metal nanoparticles and carbon-based nanomaterials for improved performances of electrochemical (bio)sensors with biomedical applications, Materials 14 (2021) 6319, https://doi.org/10.3390/ma14216319.
[36] M. Choudary, P. Yadav, A. Singh, S. Kaur, J. Ramirez-Vick, P. Chandra, K. Arora, S.P. Singh, CD 59 targeted ultrasensitive electrochemical immunosensor for fast and noninvasive diagnosis of oral cancer, Electroanalysis (2016) 28 2565–2574, https://doi.org/10.1002/elan.201600238.
[37] F. Rossi. E.H. Khoo, X. Su, N.T.K. Thanh, Study of the effect of anisotropic gold nanoparticles on plasmonic coupling with a photosensitizer for antimicrobial film, ACS Applied Biomaterials 3 (2020) 315–326, https://doi.org/10.1021/acsabm.9b00838.

[38] M. Wuithschick, A. Birnbaum, S. Witte, M. Sztucki, U. Vainio, N. Pinna, K. Rademann, F. Emmerling, R. Kraehnert, J. Polte, Turkevich in new robes: Key questions answered for the most common gold nanoparticle synthesis, ACS Nano 9 (2015) 7052−7071, https://doi.org/10.1021/acsnano.5b01579.
[39] V. Gigli, C. Tortolini, E. Capecchi, A. Angeloni, A. Lenzi, R. Antiochia, Novel amperometric biosensor based on tyrosinase/chitosan nanoparticles for sensitive and interference-free detection of total catecholamine, Biosensors 12 (2022) 519, https://doi.org/10.3390/bios12070519.
[40] W. Haiss, N.T.K. Thanh, J. Aveyard, D.G. Ferning, Determination of size and concentration of gold nanoparticles from UV-Vis spectra, Anal Chem 79 (2007) 4215−4221, https://doi.org/10.1021/ac0702084.
[41] P. Bollella, C. Schulz, G. Favero, F. Mazzei, R. Ludwig, L. Gorton, R. Antiochia, Green synthesis and characterization of gold and silver nanoparticles and their application for development of a third generation lactose biosensor, Electroanalysis 29 (2017) 77−86, https://doi.org/10.1016/j.msec.2015.04.048.
[42] K.B. Oldham, Analytical expressions for the reversible Randles-Sevcik function, J Electroanal Chem Interfacial Electroche. 105 (1979) 373–375, https://doi.org/10.1016/S0022-0728(79)80132-1.
[43] I. Lavagnini, R. Antiochia, F. Magno, An extended method for the practical evaluation of the standard rate constant from cyclic voltammetric data, Electroanalysis 16 (2004) 505–506, https://doi.org/10.1002/elan.200302851.
[44] I. Lavagnini, R. Antiochia, F. Magno, A calibration-based method for the evaluation of the detection limit of an electrochemical biosensor, Electroanalysis (2007) 19 1227–1230, https://doi.org/10.1002/elan.200703847.
[45] G. Yang, L. Li, R.K. Rana, J.J. Zhu, Assembled gold nanoparticles on nitrogen-doped graphene for ultrasensitive electrochemical detection of matrix metalloproteinase-2, Carbon 61 (2013) 357–366, https://doi.org/10.1016/j.carbon.2013.05.016.
[46] H.; Xu, H.; Ye, L.; Yu, Y.; Chi, X.; Liu, G.Chen, Tailor-made peptide sensor for detection of matrix metalloproteinase 2 in blood serum, Anal Meth 7 (2015) 5371–5374, https://doi.org/10.1039/C5AY00666J.
[47] X. Ren, T. Zhang, D. Wu, T. Yan, X. Pang, B. Du, W. Lou, Q. Wei, Increased electrocatalyzed performance through high content potassium doped graphene matrix and aptamer tri infinite amplification labels strategy: Highly sensitive for matrix metalloproteinases-2 detection Biosens Bioelectron 94 (2017) 694–700, https://doi.org/10.1016/j.bios.2017.03.064.
[48] J.J. Shi, T.T. He, F. Jiang, E.S. Abdel-Halim, J.J. Zhu, Ultrasensitive multi-analyte electrochemical immunoassay based on GNR-modified heated screen-printed carbon electrodes and PS@PDA-metal labels for rapid detection of MMP-9 and IL-6, Biosens Bioelectron 5 (2014) 51–56, https://doi.org/10.1016/j.bios.2013.11.056.
[49] G.-C. Fan, L. Han, H. Zhu, J.-R. Zhang, J.-J. Zhu, Ultrasensitive photoelectrochemical immunoassay for Matrix Metalloproteinase-2 detection based on CdS:Mn/CdTe cosensitized TiO_2 nanotubes and signal amplification of SiO_2@Ab_2 conjugates, Anal Chem 86 (2014) 12398–12405, https://doi.org/10.1021/ac504027d.
[50] H. Gao, Q. Dang, S. Xia, Y. Zhao, H. Qi, Q. Gao, C. Zhang, Highly selective electrogenerated chemiluminescence biosensor for simultaneous detection of matrix metalloproteinase-2 and matrix metalloproteinase-7 in cell secretions, Sens. Actuators B 253 (2017) 69–76, https://doi.org/10.1016/j.snb.2017.05.142.
[51] I. Ciani, H. Schulze, D.K. Corrigan, G. Henihan, G. Giraud, J.G. Terry, A.J. Walton, R. Pethig, P. Ghazal, J. Crain, C.J. Campbell, T.T. Bachmann, A.R. Mount, Development of immunosensors for direct detection of three wound infection biomarkers at point of care using electrochemical impedance spectroscopy, Biosens Bioelectron 31 (2012) 413–418, https://doi.org/10.1016/j.bios.2011.11.004.

[52] T.B. Tran, P.D. Nguyen, C. Baek, J. Min, Electrical dual-sensing method for real-time quantitative monitoring of cell-secreted MMP-9 and cellular morphology during migration process, Biosens Bioelectron 77 (2016) 631–637, https://doi.org/10.1016/j.bios.2015.10.030.
[53] E. de la Serna, E. Martínez-García, T. García-Berrocoso, A. Penalba, A. Gil-Moreno, E. Colas, J. Montaner, E. Baldrich, Using polyHRP to produce simplified immunoassays and electrochemical immunosensors, Application to MMP-9 detection in plasma and uterine aspirates, Sen. Actuators B 269 (2018)377–384, https://doi.org/10.1016/j.snb.2018.05.003.
[54] G. Ruiz-Vega, A. García-Robaina, M.B. Ismail, H. Pasamar, T. García-Berrocoso, J. Montaner, M. Zourob, A. Othmane, F.J. del Campo, E. Baldrich, Detection of plasma MMP-9 within minutes. Unveiling some of the clues to develop fast and simple electrochemical magneto-immunosensors, Biosens Bioelectron 115 (2018) 45–52, https://doi.org/10.1016/j.bios.2018.05.020.
[55] F. Jiang, J.-J. Zhang, J.-R. Zhang, J.-J. Zhu, Ultrasensitive immunoassay based on dual signal amplification of the electrically heated carbon electrode and quantum dots functionalized labels for the detection of matrix metalloproteinase-9, Analyst 138 (2013) 1962–1965, https://doi.org/10.1039/C3AN00006K.
[56] J. Lee, J.Y. Yun, W.C. Lee, S. Choi, J. Lim, H. Jeong, D.S. Shin, Y.J. Park, A reference electrode-free electrochemical biosensor for detecting MMP-9 using a concentric electrode device, Sens. Actuators B 240 (2017) 735–741, https://doi.org/10.1016/j.bios.2018.05.020.
[57] J.J. Taylor, K.M. Jaedicke, R.C. van de Merwe, S.M. Bissett, N. Landsdowne, K.M. Whall, K. Pickering, V. Thornton, V. Lawson, H. Yatsuda, T. Kogai, D. Shah, D. Athey, P.M. Preshaw, Prototype antibody-based biosensor for measurement of salivary MMP-8 in periodontitis using surface acoustic wave technology, Sci Rep 9 (2019) 11034, https://doi.org/10.1038/s41598-019-47513-w.
[58] L. Zhang, X. Li, H. Yan, L. Huang, Salivary matrix metalloproteinase (MMP)-8 as a biomarker for periodontitis: A PRISMA-compliant systematic review and meta-analysi,s *Medicine* 97 (2018) 3(e9642), https://doi.org/10.1097/md.0000000000009642.

Table 1. Comparison of electrochemical parameters before and after the modification of GPH-SPE: electroactive area (Ae, mm^2), roughness factor (ρ) and electron transfer rate constant (k_0, cm s^{-1}). Geometric area (Ag) = 11 mm^2.

GPH/SPE	ΔE/mV	Ae/mm^2	ρ	k_0/10^{-3} cm s^{-1}
bare	93	13	1.5	2.05 ± 0.13
GNPs	92	18	1.64	2.18 ± 0.19
AuNSs	90	23	2.09	2.68 ± 0.21
11-MUA/AuNSs	254	10	0.91	1.93 ± 0.15
anti-MMP-8/BSA/11-MUA/AuNSs	253	8	0.73	1.59 ± 0.19

Table 2. Parameters for Randles model on bare and modified GPH-SPE.

SPE	R_{CT} (Ω)	CPE (μMho*s^N)	N	W (mMho $s^{1/2}$)
bare	360	63.2	0.667	0.77
GNP	349	30.1	0.740	1.16
AuNSs	164	3.81	0.696	1.72
11-MUA/AuNSs	546	1.83	0.655	1.11
anti-MMP-8/BSA/11-MUA/AuNSs	717	1.49	0.645	1.03
MMP-8/anti-MMP-8/BSA/11-MUA/AuNSs	1560	2.73	0.918	1.77

Table 3. Comparison with other electrochemical and piezoelectric biosensors for MMPs reported in literature.

List of abbreviations: NG: Nitrogen-doped graphene sheet; PDA: polydopamine; GO: graphene oxide; HRP: horseradish peroxidase; depAu: electrodeposition of gold nanoparticles; GCE: glassy carbon electrode; NPs: nanoparticles; pPtNPs: porous platinum nanoparticles; P1: peptide; Pep: peptide; Fc: ferrocenylacetic acid; PSC: polystyrene microsphere; SA: streptavidin; Thi: thionine; mhCeO2NS: mesoporous-hollow ceria nanospheres; GS graphene sheets; PSt: Polystyrene spheres; NTs: nanotubes; CB[7]:cucurbit[7]uril; Fc-HRP/Fc-GOx: ferrocene-labeled HRP and ferrocene-labeled glucose oxidase (GOx); QDs: quantum dot; SiNW: Silicium nanowires; rGO: reduced graphene oxide; MB: methylene blue; SAH: sodium alginate hydrogel; SAM: self-assembled monolayer of $HS(CH_2)_{11}COOH$; GNR: graphene nanoribbon; HSPCE: heated screen-printed carbon electrode; :IDAMs: interdigitated array microelectrodes; PS: polyethylene sphere; CA: cysteamine hydrochloride; Abs: antibodies; DPV: differential potential voltammetry; ChA: Chronoamperometry; SWV: square wave voltammetry; PEC: photoelectrochemical immunoassay; ASV: anodic stripping voltammetry; ECL: electrochemiluminescence; FET: Field-Effect Transistor; EIS: electrochemical impedance spectroscopy; SAW: Surface Acoustic wave.

MMP	Sensing Platform	Signal Transductor	Linear Range/ng mL^{-1}	LOD/ng mL^{-1}	Sample	Ref.
MMP-2	Au-NG/PDA-GO-HRP	DPV	0.5 10^{-3} ÷ 50	0.11 10^{-3}	PBS	**[45]**
	depAu/GCE-S-pPtNPs-P1	DPV	1 10^{-3} ÷ 10	0.32 10^{-3}	PBS	**[22]**
	Au electrode-Pep-Fc	DPV	100 10^{-3} ÷ 200	0.3	human serum	**[46]**
	PSC-Pep-AuNPs-DNA 1	DPV	0.5 10^{-3} ÷ 50	0.15 10^{-3}	human serum	**[23]**
	SA/Thi/Pt/Pd/mhCeO_2NS	DPV	0.1 10^{-3} ÷ 10	0.08 10^{-3}	human serum	**[24]**
	K-GS/aptamer	ChA	10^{-4} ÷ 10	35 10^{-6}	human serum	**[47]**
	PSt@PDA-AgNPs	SWV	10^{-5} ÷ 1000	5 10^{-6}	human serum	**[48]**
	TiO_2-NTs/CdS:Mn/CdTe	PEC	10 10^{-6} ÷ 500 10^{-3}	3.6 10^{-6}	-	**[49]**
	PtNPs@CB[7]/Fc-HRP/Fc-GOx	DPV	0.1 10^{-3} ÷ 20	0.03 10^{-3}	human serum	**[25]**
	Au-QDs core-satellite nanoprobes	ASV	1 10^{-3} ÷ 500 10^{-3}	0.03 10^{-6}	human serum	**[26]**
	Au electrode-Pep-Ru1	ECL	10÷ 300	5	living cells	**[50]**
	SiNW-peptide	FET	1.4 10^{-5} ÷ 1.4 10^{-3}	1.4 10^{-5}	-	**[27]**
	SiNW-peptide-DNA-AuNPs	FET	1.4 10^{-9} ÷ 0.14 10^{-3}	1.4 10^{-9}	PBS, human plasma	**[32]**
MMP-3	SWCNT/polybeads	ChA	4 10^{-3} ÷ 300 10^{-3}	4 10^{-3}	calf serum	**[33]**
MMP-7	Fc-peptide-Au electrode	SWV	0.1 ÷ 10	0.07	Tricine buffer	**[28]**
	Au electrode-Pep-Fc	SWV	-		cells	**[19]**
	Au-rGO/MB-SAH-Pd-SAM-PDA	SWV	10 10^{-6} ÷10	3.1 10^{-6}	healthy human serum	**[29]**

	depAu/GCE	SWV	$0.1\ 10^{-3} \div 50$	$0.02\ 10^{-3}$	-	**[30]**
	depAu/GCE-S-pPtNP-P1	DPV	$0.2\ 10^{-3} \div 20$	$0.05\ 10^{-3}$	-	**[31]**
	Au electrode-Pep-Ir1	ECL	$0.05 \div 1$	$10\ 10^{-3}$	living cells	**[50]**
	rGO-peptide	FET	$10 \div 1\ 10^{3}$	10	-	**[32]**
MMP-9	SAM-Au macrodisc electrode	EIS	-	100	mock wound fluid	**[51]**
	Au electrode-Pep-MB	SWV	$5.58 \div 4650$	5.58	PBS	**[19]**
	GNR/HSPCE	SWV	$10\ 10^{-6} \div 1\ 10^{3}$	$5\ 10^{-6}$	PBS	**[48]**
	IDAMs	Capacitive	$0.93 \div 930$	0.93	MCF-7 cells in PBS	**[52]**
	MB/poly-HRP	ChA	$30\ 10^{-3} \div 1000\ 10^{-3}$	$18\text{-}28\ 10^{-3}$	human plasma / uterine aspirates	**[53]**
	MB/poly-HRP	ChA	$0.03 \div 2$	$13\ 10^{-3}$	human plasma	**[54]**
	PS@PDA/CdTe-QDs	DPV	$0.3\ 10^{-3} \div 10$	$0.033\ 10^{-3}$	human serum	**[55]**
	Au electrode-Pep-MB	CV	$0.093 \div 93$	0.65	PBS	**[56]**
	Au/Pep-hydrogel/dextran/CA	EIS	$50 \div 400$	15	Tris buffer	**[20]**
	MoS_2-$A\beta_{1-42}$	FET	$0.093 \div 930$	0.093	MCF-7 cells	**[21]**
MMP-8	anti-MMP-8/BSA/11-MUA/AuNSs/GPH/SPE	DPV	2.5-300	1	PBS, saliva	**this work**
	Specific-Abs biochip	SAW	$0 \div 1000$	62.5	saliva	**[57]**

Table 4. MMP-8 determination in human saliva samples using the proposed immunosensor and a conventional ELISA assay.

Saliva Sample	Oral health status	MMP-8 immunosensor (ng mL^{-1})	MMP-8 ELISA assay (ng mL^{-1})	RSD%	Periosafe ® Test
patient 1	health	52.6	48.1	8.6	-
patient 2	health	26.1	28.0	6.8	-
patient 3	health	74.8	80.3	6.9	-
patient 4	health	95.1	107.7	11.7	-
patient 5	health	66.7	73.6	9.4	-
patient 6	gingivitis	229.2	201.2	12.3	+
patient 7	gingivitis	348.1	365.0	4.7	+
patient 8	gingivitis	129.7	141.2	8.2	+
patient 9	periodontitis	672.0	589.3	12.4	+
patient 10	periodontitis	888.5	956.2	7.1	+

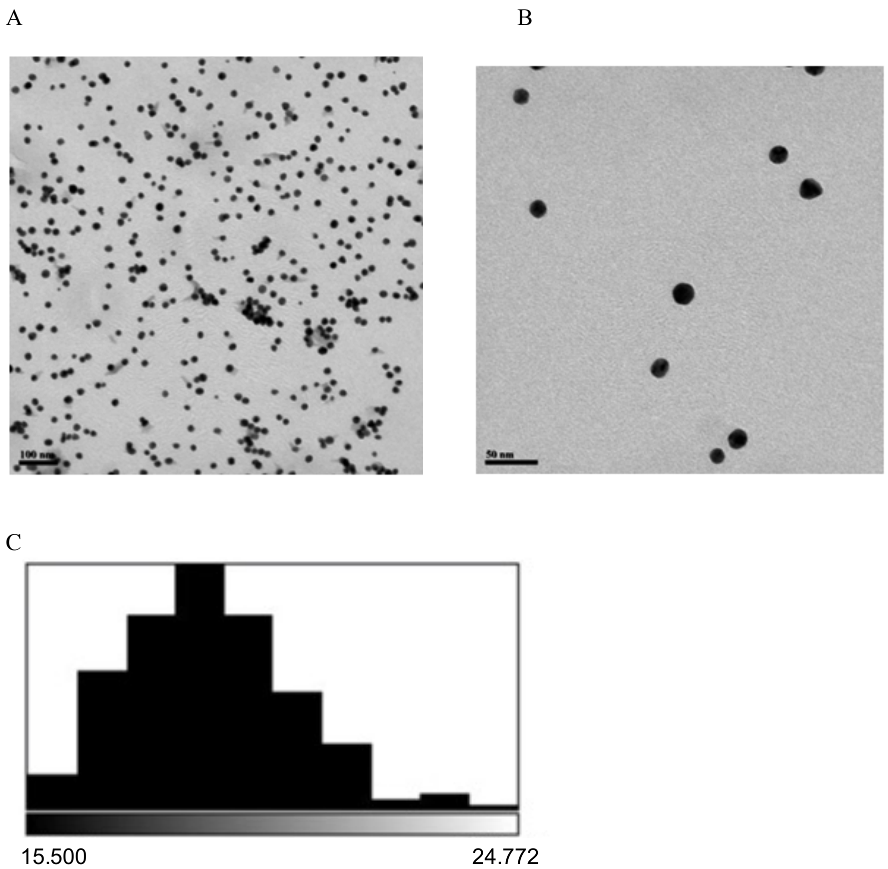

Fig. 1. TEM images of AuNSs at the following magnification: 10.000X (A) and 30.000X (B) and (C) histogram analysis of particle size distribution.
Count: 200; mean 18.908; SD: 1.581; bins: 10; min: 15.500; max: 24.772; mode: 18.282 (48); bin width: 0.927.

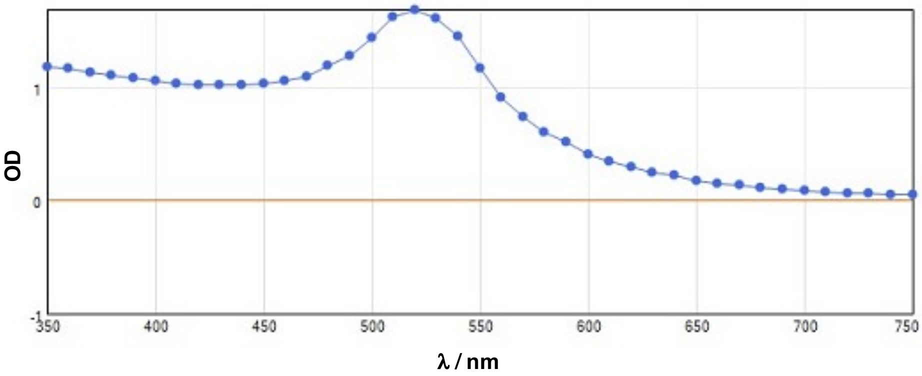

Fig. 2. UV-Vis spectra of a colloidal solution of AuNSs in water.

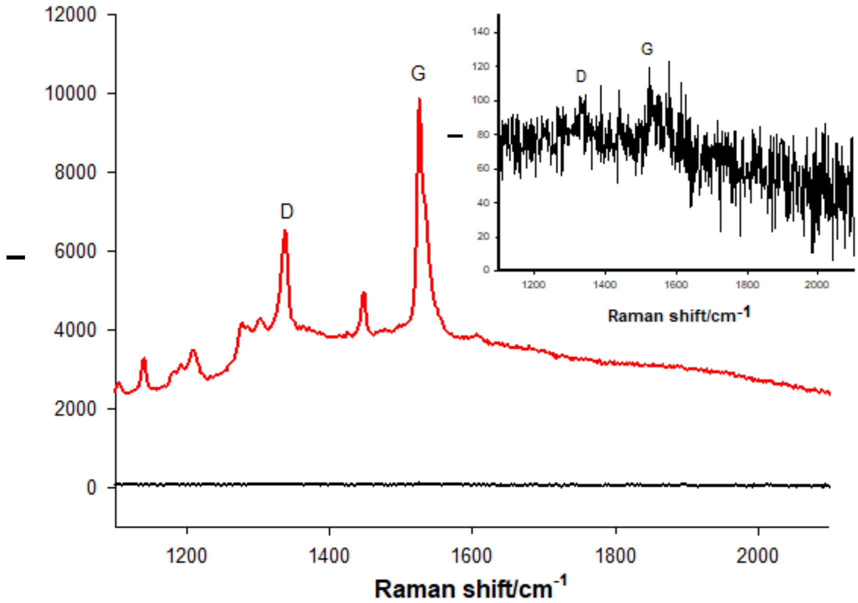

Fig.3. Raman spectra of GPH-SPE (black) and modified AuNSs-GPH-SPE.

A

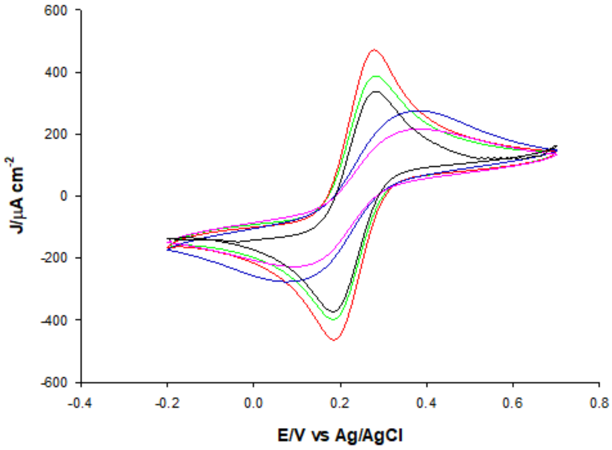

B

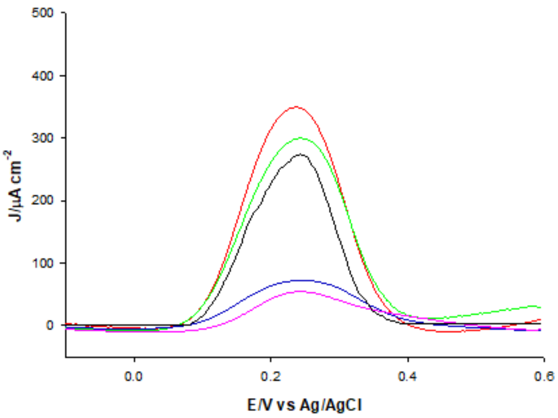

Fig. 4. (A) CVs at 25 mV s^{-1} (A) and DPVs (B) of bare (black), GNPs (green), AuNSs (red), 11-MUA/AuNSs (blue) and anti-MMP-8/BSA/EDC-NHS/11-MUA/AuNSs (pink) GPH/SPE in Zobell's solution.

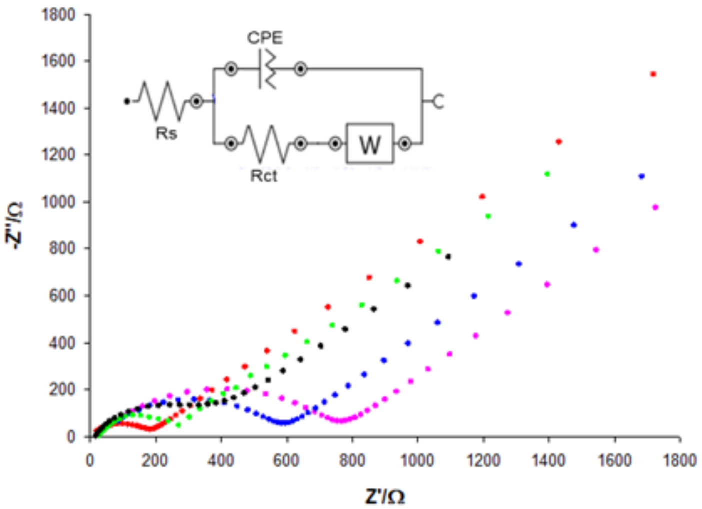

Fig.5. Nyquist plot of bare (black), GNPs (green), AuNSs (red), 11-MUA/AuNSs (blue) and anti-MMP-8/BSA/EDC-NHS/11-MUA/AuNSs (pink) GPH/SPE in Zobell's solution. Frequency measured from 10^{-1} Hz to 10^{5} Hz, with amplitude of 10 mV, potential applied at + 0.167 V.

A

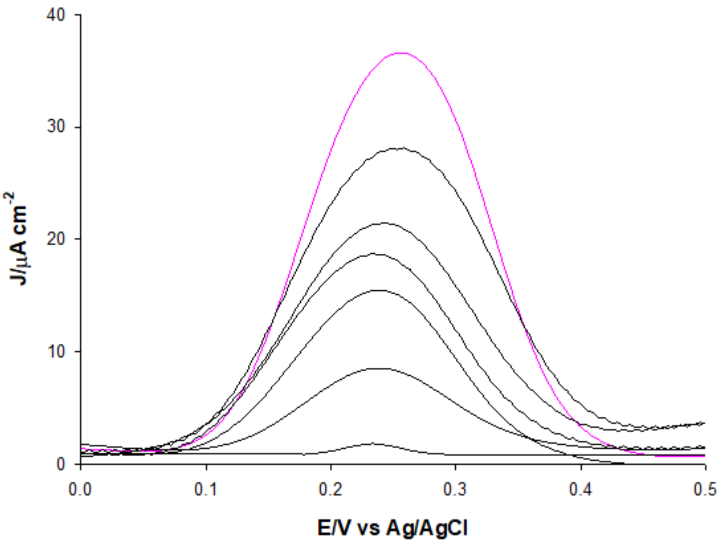

B

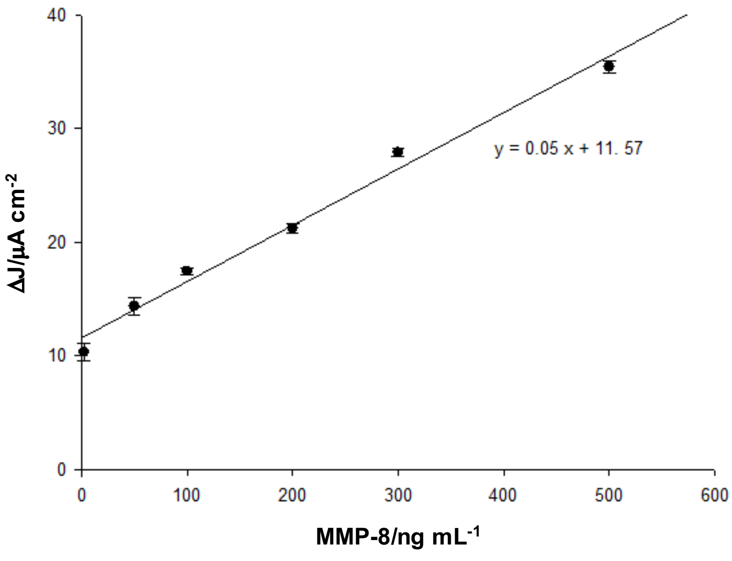

Fig. 6. (A) Typical DPV of immunosensor at increasing MMP-8 (2.5, 50, 100, 200, 300, 500 ng mL^{-1} in Zobell's solution, black curves; the pink curve is relative to the anti-MMP-8 without MMP-8

antigen; (B) Calibration curve of the MMP-8 immunosensor at increasing MMP-8 concentrations (2.5, 50, 100, 200, 300, 500 ng mL^{-1} in Zobell's solution). R^2=0.986.

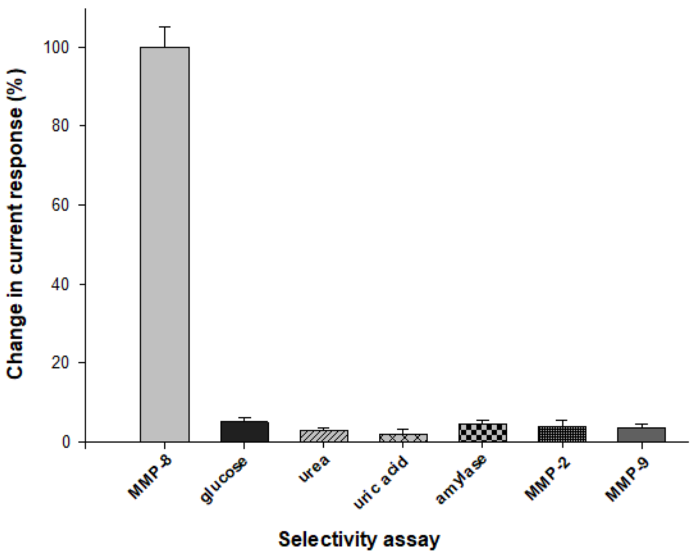

Fig. 7. Histograms of selectivity assay for MMP-8 vs. different interferent proteins in Zobell's solution.

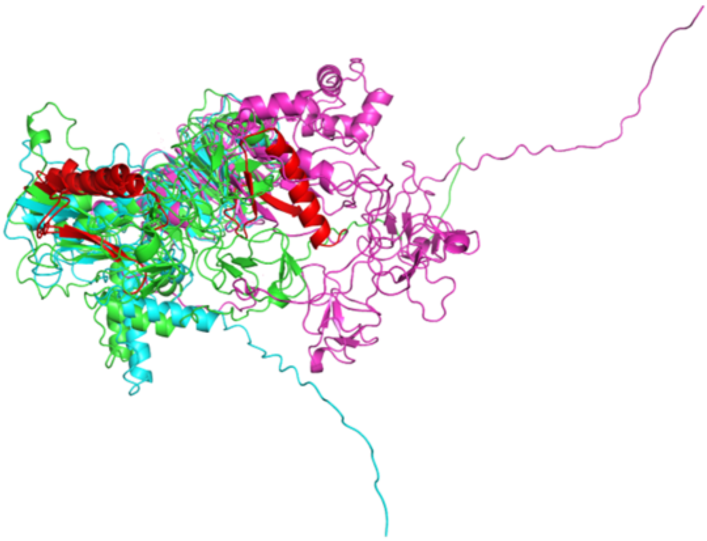

Fig. 8. Superposition in carton ribbons of the MMP-8 (green), MMP-2 (cyano) and MMP-9 (magenta) structures (using AlfaFold coordinates). The target regions are colored in red.